• Basic Research •

FLNA promotes the progression of diabetic retinopathy by increasing M1 macrophages

Chun-Hua Li[1], *Mao-Fei Feng*[2], *Xue Zhang*[1], *Lei Yu*[1]

[1]Xi'an People's Hospital (Xi'an Fourth Hospital), Shaanxi Eye Hospital, Affiliated Guangren Hospital, School of Medicine, Xi'an Jiaotong University, Xi'an 710000, Shaanxi Province, China

[2]Wuzhong People's Hospital, Wuzhong 215128, Ningxia Hui Autonomous Region, China

Correspondence to: Xue Zhang. Xi'an People's Hospital (Xi'an Fourth Hospital), Shaanxi Eye Hospital, Affiliated Guangren Hospital, School of Medicine, Xi'an Jiaotong University, No.155 Aerospace East Road, Chang'an District, Xi'an 710000, Shaanxi Province, China. Zhangxue0927@163.com

Received: 2026-01-13 Accepted: 2026-05-07

Abstract

● **AIM:** To clarify the role of filamin A (FLNA) in promoting diabetic retinopathy (DR) progression and explore its underlying mechanism *via* modulating M1 macrophage inflammation and adenosine 5'-monophosphate activated protein kinase (AMPK) phosphorylation, as well as its potential as a diagnostic biomarker and therapeutic target.

● **METHODS:** Gene Expression Omnibus (GEO) dataset and Weighted Gene Co-Expression Network Analysis (WGCNA) were used to identify differentially expressed genes across DR, diabetes mellitus (DM), and control groups. Gene Set Enrichment Analysis (GSEA), Gene Ontology (GO), and Kyoto Encyclopedia of Genes and Genomes (KEGG) were employed to analyze the enrichment of intersecting genes. Machine learning models assessed the predictive performance of these genes, while single-cell sequencing and cell chat examined their expression in M1 macrophages and interactions with other cell types. Quantitative PCR (q-PCR) measured mRNA levels of interleukin- 6 (IL-6), interleukin-1β (IL-1β), and tumor necrosis factor-α (TNF-α), and Western blotting assessed protein levels of FLNA, AMPK, and phosphorylated-AMPK (p-AMPK).

● **RESULTS:** Key findings revealed *FLNA*, plectin (*PLEC*), and Tweety family member 3 (*TTYH3*) as critical genes in DR, with *FLNA* showing the highest area under the curve (AUC) value and importance, and the random forest model performing best. The AMPK signaling pathway was enriched for FLNA, which was most significantly expressed in M1 macrophages. M1 macrophages promote IL-6, IL-1β, and TNF-α expression. FLNA increases the effect of M1 macrophages on DR progression and AMPK phosphorylation.

● **CONCLUSION:** Our study identifies FLNA as a key regulator in DR progression, primarily by enhancing M1 macrophage-mediated inflammation and AMPK phosphorylation. These findings highlight FLNA's critical role in DR pathogenesis and its potential as a biomarker for early diagnosis and a therapeutic target for intervening in macrophage-driven inflammatory responses.

● **KEYWORDS:** diabetic retinopathy; M1 macrophages; machine learning; FLNA; phosphorylated-AMPK

DOI:10.18240/ijo.2026.09.04

Citation: Li CH, Feng MF, Zhang X, Yu L. FLNA promotes the progression of diabetic retinopathy by increasing M1 macrophages. *Int J Ophthalmol* 2026;19(9):1687-1699

INTRODUCTION

Diabetic retinopathy (DR) stands as the leading cause of blindness among working-age adults worldwide, with its global prevalence projected to reach 160 million by 2045[1]. Clinically, DR is categorized into non-proliferative diabetic retinopathy (NPDR) and proliferative diabetic retinopathy (PDR), characterized by microvascular leakage, diabetic macular edema (DME), and pathological neovascularization[2-3]. Although anti-vascular endothelial growth factor (anti-VEGF) agents, including ranibizumab and aflibercept, have substantially improved clinical outcomes, approximately 40%–50% of patients exhibit suboptimal response[4]. Moreover, frequent intravitreal injections pose considerable challenges, including poor patient compliance, risk of retinal fibrosis, and endophthalmitis[5]. Emerging therapeutic modalities, such as complement inhibitors and gene therapies, have entered clinical trials but demonstrated limited efficacy[6-9]. Consequently, elucidating novel pathogenic mechanisms and developing targeted interventions remain imperative.

DR is fundamentally a chronic low-grade inflammatory disorder, with macrophage polarization imbalance serving

as the critical node in this inflammatory cascade[10-11]. Macrophages, as principal effector cells of innate immunity, exhibit remarkable plasticity, differentiating into pro-inflammatory M1 or anti-inflammatory M2 phenotypes under distinct microenvironmental cues[12-13]. M1 macrophages, induced by interferon gamma (IFN-γ), lipopolysaccharide (LPS), or hyperglycemia, highly express inducible nitric oxide synthase (iNOS), cluster of differentiation 86 (CD86), and pro-inflammatory cytokines [tumor necrosis factor (TNF)-α, interleukin (IL)-1β, IL-6, IL-12], driving Th1 immune responses. Conversely, M2 macrophages, polarized by IL-4 and IL-13, express arginase-1 (Arg-1), CD206, and anti-inflammatory mediators such as IL-10 and transforming growth factor beta (TGF-β), facilitating tissue repair and inflammation resolution[14]. Recent single-cell transcriptomic analyses have revealed multiple macrophage subpopulations in the retina, including microglia and infiltrating monocyte-derived macrophages, which display heterogeneous polarization signatures across different DR stages[15-16]. In vitreous and retinal tissues from DR patients, the M1/M2 ratio is markedly skewed toward M1 dominance, correlating positively with disease severity[17]. Experimental studies have demonstrated that macrophage depletion or induction of M2 repolarization attenuates retinal vascular leakage and neovascularization[18-19]. Thus, modulating macrophage polarization represents a promising therapeutic strategy for DR.

This study aims to utilize clinical information datasets of DR, diabetes mellitus (DM), and control groups obtained from the Gene Expression Omnibus (GEO) database, followed by performing differential expression analysis and Weighted Gene Co-expression Network Analysis (WGCNA) analysis to identify key intersecting genes associated with DR. Based on these intersecting genes, a risk prediction model for DR will be constructed and evaluated. Additionally, single-cell analysis will be conducted on the GSE dataset to identify the most closely related cell types to DR and the intersecting genes. We have identified filamin A (FLNA) which is closely associated with macrophages in the disease process of DR. FLNA, an actin-crosslinking cytoskeletal protein, has emerged as a critical mediator of mechanotransduction and signal transduction in vascular endothelial cells[20-21]. FLNA interacts with adenosine 5'-monophosphate (AMP)-activated protein kinase (AMPK), a master regulator of cellular energy metabolism and inflammation[22]. Furthermore, *in vitro* cell experiments performed to validate the role and underlying mechanisms of FLNA and M1 macrophages in DR (Figure 1). Recent evidence indicates that FLNA editing in myeloid cells governs resistance to inflammation by reducing macrophage production of IL-6, IL-1β, and TNF-α[23]. In diabetic contexts, AMPK phosphorylation can either protect against metabolic stress or, paradoxically, drive inflammatory mitophagy depending on the cellular context[23]. The AMPK/mTORC1 axis dynamically counterbalances M1 and M2 macrophage polarization, with AMPK activation favoring the M2 reparative phenotype, whereas mTORC1 signaling promotes the M1 pro-inflammatory state[22]. This study aims to fill this gap by integrating bulk and single-cell transcriptomics with machine learning and experimental validation.

MATERIALS AND METHODS

Data Collection Transcriptomic data related to human DR were obtained from the publicly accessible GEO database (https://www.ncbi.nlm.nih.gov/geo/). GSE221521 (platform: GPL24676) is a bulk expression dataset containing 50 normal control samples (Control), 69 DR samples, and 74 DM samples. GSE243100 (platform: GPL24247) is a mouse single cell dataset containing 2 normal control samples and 2 DR samples.

Identification of M1-related Differentially Expressed Genes in DR Using the R program (version 4.2.1) "limma", we evaluated DEGs between DR and control subjects, as well as between DR and DM, in GSE221521. Statistical significance was determined by a $|\log_2 \text{fold change}|>1$ and an adjusted $P<0.05$ (Benjamini-Hochberg method). We also evaluated immune cell abundance in GSE221521 using the Xcell (version 1.1.0) algorithm in the Immune Oncology Biological Research (IOBR, version 2.0.0+) and compared immune cell abundance between DR and control subjects. Using M1 macrophage abundance as a phenotype, we used WGCNA (version 1.72-1) to identify key modules (Soft Thresholding Power=6). Genes with a GS>0.4 and MM>0.6 within the key modules were considered key genes. By overlapping DEGs with genes in the WGCNA key modules, we identified M1 macrophage-related genes in DR.

Identification of Key Genes and Construction of Risk Prediction Models To identify the optimal model-building strategy, we used the aforementioned key genes and benchmarked the "Logistic", RandomForest, XGBoost, SVM, and NeuralNet algorithms from mlr3verse (version 0.2.7). We selected the optimal model algorithm based on metrics such as area under the curve (AUC), accuracy, and F1 to construct the risk model. Based on the predicted probability of the optimal model, we calculated a risk score for each sample and normalized the risk score to a scale of 1–100. Model performance was evaluated using receiver operating characteristic (ROC) curves (pROC), direct current analysis (DCA) curves (ggDCA), and calibration curves. Internal validation was performed using booststrap=2000.

Functional Enrichment Analysis Kyoto Encyclopedia of Genes and Genomes (KEGG) gene sets were acquired and processed through clusterProfiler, retaining those with member counts between 15 and 500. Enrichment significance

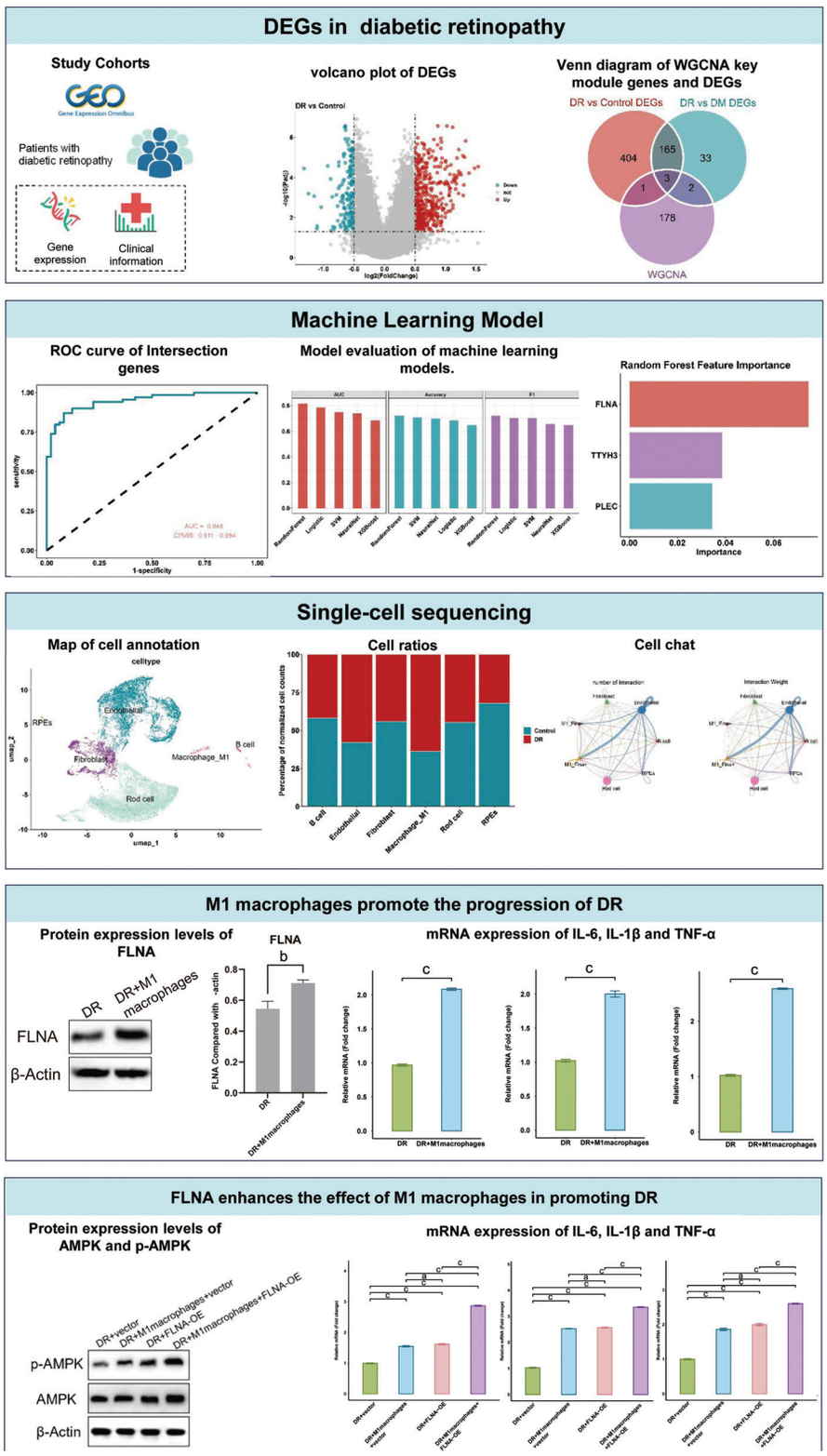

Figure 1 Experimental flow chart of the study DR: Diabetic retinopathy; DEGs: Differentially expressed genes; ROC: Receiver operating characteristic; FLNA: Filamin A; IL: Interleukin; TNF: Tumor necrosis factor; AMPK: AMP-activated protein kinase. [a]*P*<0.05, [b]*P*<0.01, [c]*P*<0.001.

was assessed *via* 100 permutation tests ($P<0.05$). For DEGs across risk-based groups, Gene Ontology (GO) and KEGG enrichment was evaluated. Results were deemed significant under the following criteria: false discovery rate (FDR)<0.05, adj$P$<0.05, and Q value<0.05, following Benjamini-Hochberg adjustment (BH).

Single-cell Data Analysis scRNA-seq data analysis was performed using Seurat (version 4.3.0). After quality control exclusion of cells with mitochondrial (<5%), ribosomal (>20%), or erythroid (>3%) gene contamination, the dataset underwent normalization and variable gene selection. Scaled variable genes were subjected to principal component analysis (PCA),

Table 1 List of primers of qPCR

Gene	Forward (5′-3′)	Reverse (5′-3′)
IL-6	CCACTTCACAAGTCGGAGGCTTA	GCAAGTGCATCATCGTTGTTCATAC-
TNF-α	GGTGCCTATGTCTCAGCCTCTT	GGTGCCTATGTCTCAGCCTCTT
IL-1β	TCCTGTCTTGGCCGAGGACTAAGG	TC TGGGCTGGACTGTTTCTAATGC

IL: Interleukin; TNF: Tumor necrosis factor; qPCR: Quantitative real-time polymerase chain reaction.

followed by cellular clustering through neighbor finding and cluster detection functions. Final cell type identification was accomplished using the CellMarker (version 2.0) repository.

Cell Communication Analysis We used Cell Chat (version 1.6.1) to investigate the molecular interaction networks between different cell types in tumor tissues. Ligand-receptor pairs with a *P*-value less than 0.05, as determined by Cell Chat, were considered to be significant interactors between different cell subpopulations.

Establishment of DR Cell Model Human retinal microvascular endothelial cells lines (HRMECs) used in this study were obtained commercially from the American Type Culture Collection (ATCC, Manassas, VA, USA; Catalog No. PCS-100-022). HRMECs were cultured in DMEM (Gibco 11965092) supplemented with 10% (v/v) fetal bovine serum (FBS, Gibco 10099141C) and 1% (v/v) penicillin-streptomycin (Gibco 15140122) incubated at 37℃ in a 5% CO_2 atmosphere. Culture medium was refreshed every 2d, and cells were passaged at 80%–90% confluence using 0.25% trypsin-EDTA (Gibco 25200056). For high glucose (HG) treatment, cells at 70%–80% confluence were serum-starved in DMEM with 1% FBS for 12h, then exposed to 30 mmol/L D-glucose (Sigma G8270, freshly prepared, osmolality adjusted to ~330 mOsm/kg with mannitol to control for osmotic stress) for 96h. Normal glucose (NG) control used 5 mmol/L D-glucose with 25 mmol/L mannitol (Sigma M4125) as osmotic control. Cells from passages 3-6 were used for all experiments to minimize senescence-related variability.

RNA Extraction and Quantitative Real-Time Polymerase Chain Reaction Cell samples were collected post-treatment and homogenized in Trizol (Invitrogen 15596018). Following a 5-minute room temperature incubation and centrifugation, chloroform was added, and the mixture was shaken vigorously before resting for 2–3min. After another centrifugation step, the aqueous phase was recovered, and isopropanol was added to precipitate RNA. After 10min of incubation and centrifugation, the RNA pellet was collected, washed twice with 75% ethanol, and dried. The purified RNA was dissolved in RNase-free water (Invitrogen 10977015). RNA concentration and purity were assessed by multiscan spectrum (Thermo Fisher Varioskan LUX).

Reverse transcription was performed using the PrimeScript RT Reagent Kit (Takara RR047). Quantitative real-time polymerase chain reaction (qPCR) was conducted on a QuantStudio 3 Real-Time PCR System (Applied Biosystems) using TB Green Premix Ex Taq II (Takara RR820A). Cycling conditions: 95℃ for 30s; 40 cycles of 95℃ for 5s, 60℃ for 30s; followed by melt curve analysis. Using the primers provided in Table 1, perform the amplification of PCR primers. All samples were run in triplicate technical replicates. Three independent biological replicates were performed for each experimental condition (n=3). Relative mRNA expression was calculated using the $2^{-\Delta\Delta Ct}$ method with GAPDH as the internal reference. Amplification efficiency for all primer pairs was validated by standard curve analysis (R^2>0.98). Melt curve analysis confirmed single-product amplification. Data analysis is conducted by Graph Pad.

Western Blotting The collected cells were lysed and the proteins were extracted. The protein concentration was detected using a BCA kit (Beyotime P0012S) according to the instructions, and the sample loading system was prepared by adding triple-distilled water and buffer. The sample loading system was added to the pre-prepared gel (Epizyme LK403) for electrophoresis stratification. The electrophoresis time was adjusted according to the Maker (epizyme WJ103) stratification. After the electrophoresis, the proteins in the gel were transferred to the PVDF membrane (Millipore 03010040001). The bands were blocked with skim milk powder (Beyotime P0216), washed with TBST (zhhcbio HT106). After blocking, membranes were incubated with primary antibodies against FLNA (Abcam ab76289 1:1000), AMPK (Abcam ab32047 1:1000), p-AMPKα (Abcam ab131357 1:500) and GAPDH (Proteintech 60004-1-Ig 1:1000). After washing, the blots were incubated with HRP-conjugated anti-rabbit (1:5000; Jackson ImmunoResearch, 111-035-003) and anti-mouse (1:5000; Jackson ImmunoResearch, 115-035-003) secondary antibodies. The samples were developed using enhanced chemiluminescence (ECL, epizyme SQ202) in a chemiluminescence system (BIORED ChemiDoc MP) and photographed. Each Western blot experiment included three independent biological replicates per group (n=3). Data analysis is conducted by Graph Pad and ImageJ.

Data Analysis R v4.2.1 was used for all statistical analyses. One-way analysis of variance (ANOVA) or Student's *t*-tests were used to compare results between groups. Pearson correlation coefficients were used to assess relationships

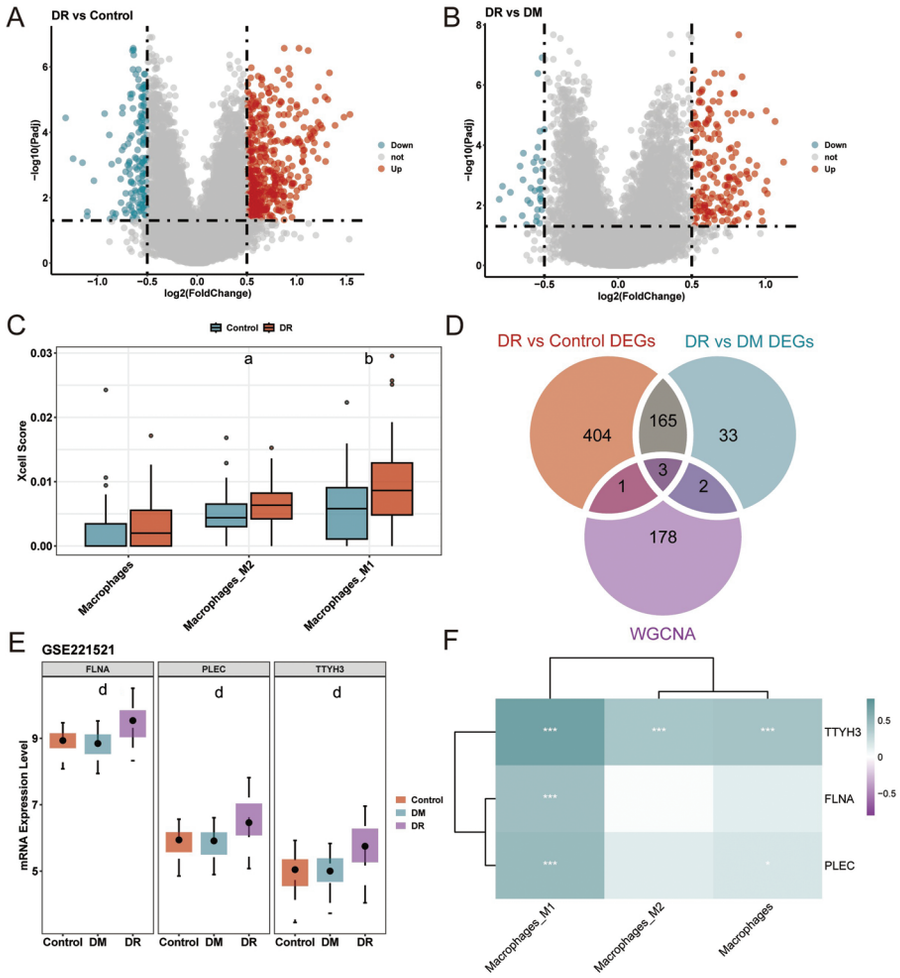

Figure 2 Analysis of differentially expressed genes in DR A: Volcano plot of differential expression of DR *vs* control; B: Volcano plot of differential expression of DR *vs* DM; C: Boxplot of differential expression between DR and control groups in macrophages; D: Venn diagram of the intersection of Weighted Gene Co-Expression Network Analysis (WGCNA) key module genes and differentially expressed genes (DEGs); E: mRNA expressionn levels of intersection genes in control, DM and DR; F: Correlation between intersection gene expression and macrophage abundance. [a]*P*<0.05, [b]*P*<0.01, [d]*P*<0.0001. DR: Diabetic retinopathy; DM: Diabetes mellitus.

between variables, with an *r* value of 0.3 considered significant. A *P* value of less than 0.05 was considered critical for significance.

RESULTS

Analysis of Differentially Expressed Genes in Diabetic Retinopathy We analyzed a single-cell RNA sequencing dataset (GSE243100) containing normal control and DR samples, as well as a bulk RNA sequencing dataset (GSE221521) comprising DR and DM samples, performing differential expression analysis on both datasets (Figure 2A–2B). Subsequently, we assessed the abundance of immune cells in DR and control groups, revealing stronger immune cell infiltration in the DR group. Notably, there was a significant difference in macrophage abundance between the control and DR groups. To further investigate the expression differences in macrophages between the control and DR groups, we analyzed the expression levels of different macrophage subsets in the GSE243100 dataset. The results showed that both groups exhibited the highest expression levels in M1 macrophages, with significant differences in expression between the two groups (Figure 2C). By performing WGCNA on the GSE221521 dataset, we identified key gene modules. The intersection analysis of these module genes with the differentially expressed genes from both GSE243100 and GSE221521 datasets revealed three key genes associated with DR: FLNA, plectin (PLEC), and Tweety family member 3 (TTYH3; Figure 2D). The mRNA expression levels of these three genes across different groups indicated that FLNA had the highest expression, and all three genes were significantly upregulated in the DR group compared to the DM and control groups (Figure 2E). Furthermore, the correlation analysis of these genes' expression levels with macrophage abundance demonstrated that all three genes were significantly more highly expressed in M1 macrophages compared to M2 macrophages and macrophages overall, with TTYH3 showing the highest significance (Figure 2F). These findings suggest that these DR-associated genes are highly expressed in M1

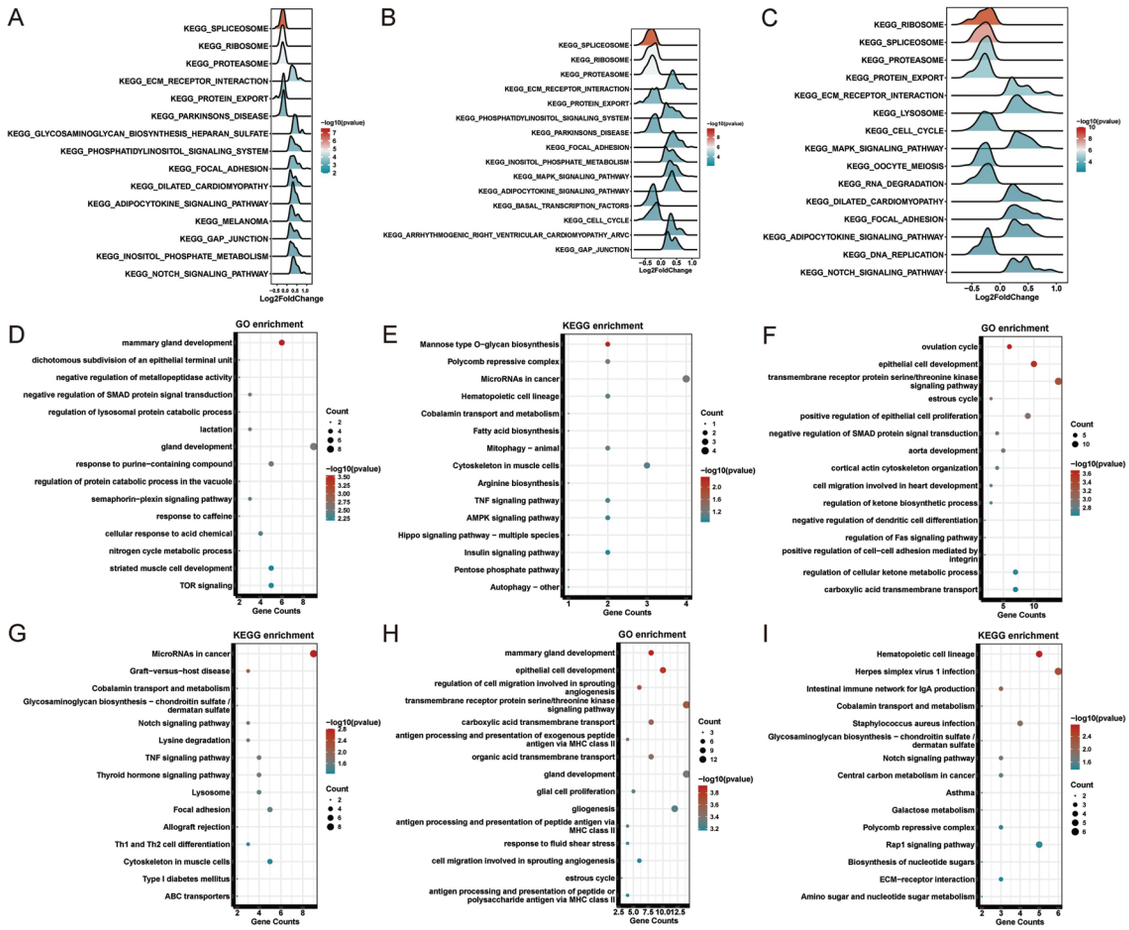

Figure 3 Functional enrichment analysis of intersection genes Gene Set Enrichment Analysis (GSEA) enrichment analysis of filamin A (FLNA; A), plectin (PLEC; B), and Tweety family member 3 (TTYH3; C). Gene Ontology (GO; D) and Kyoto Encyclopedia of Genes and Genomes (KEGG; E) enrichment analysis of FLNA. GO (F) and KEGG (G) enrichment analysis of PLEC. GO (H) and KEGG (I) enrichment analysis of TTYH3.

macrophages, implying that M1 macrophages may play a role in DR progression.

Functional Enrichment Analysis of Intersection Genes Through Gene Set Enrichment Analysis (GSEA), as well as GO and KEGG enrichment analysis, we explored the potential functions and regulatory signaling pathways of the intersection genes. The GSEA results revealed that the potential functions and signaling pathways of the three intersection genes exhibited notable overlap, with key enriched functions including Spliceosome, Ribosome, and Focal_Adhesion, and major enriched signaling pathways such as the Phosphatidylinositol_Signaling_System and Notch_Signaling_Pathway (Figure 3A–3C). GO and KEGG analyses further indicated that FLNA is associated with functions and pathways such as mammary gland development, striated muscle cell development, mannose type O-glycan biosynthesis, TNF signaling pathway, and AMPK signaling pathway (Figure 3D–3E). PLEC and TTYH3 were found to be linked to pathways and processes including the transmembrane receptor protein serine/threonine kinase signaling pathway, epithelial cell development, graft-versus-host disease, and Notch signaling pathway (Figure 3F–3I). Additionally, ROC curve analysis demonstrated that FLNA and TTYH3 exhibited good predictive performance for DR, with AUC values of 0.77 and 0.778, respectively, while PLEC showed relatively lower predictive efficiency with an AUC value of 0.755.

Multiple Machine Learning for Intersection Genes The initial results suggest that the intersection genes have predictive potential for DR. To further validate the role of the intersection genes in DR, we conducted a comprehensive evaluation of their predictive performance using machine learning models. After assessing various models, including Logistic Regression, Random Forest, Support Vector Machine (SVM), XGBoost, and Neural Network, we found that Random Forest consistently demonstrated the best performance in terms of sensitivity (AUC), accuracy, and reliability (F1; Figure 4A, Table 2). Therefore, we selected Random Forest as the optimal model to construct a risk score and validated it in the testing set (Figure 4B). We also ranked the importance of the intersection genes, revealing that FLNA was the most significant, followed by TTYH3, and then PLEC (Figure 4C–4D). Furthermore, as expected, the risk score distribution in the GSE221521 dataset showed significantly higher scores in the DR group compared

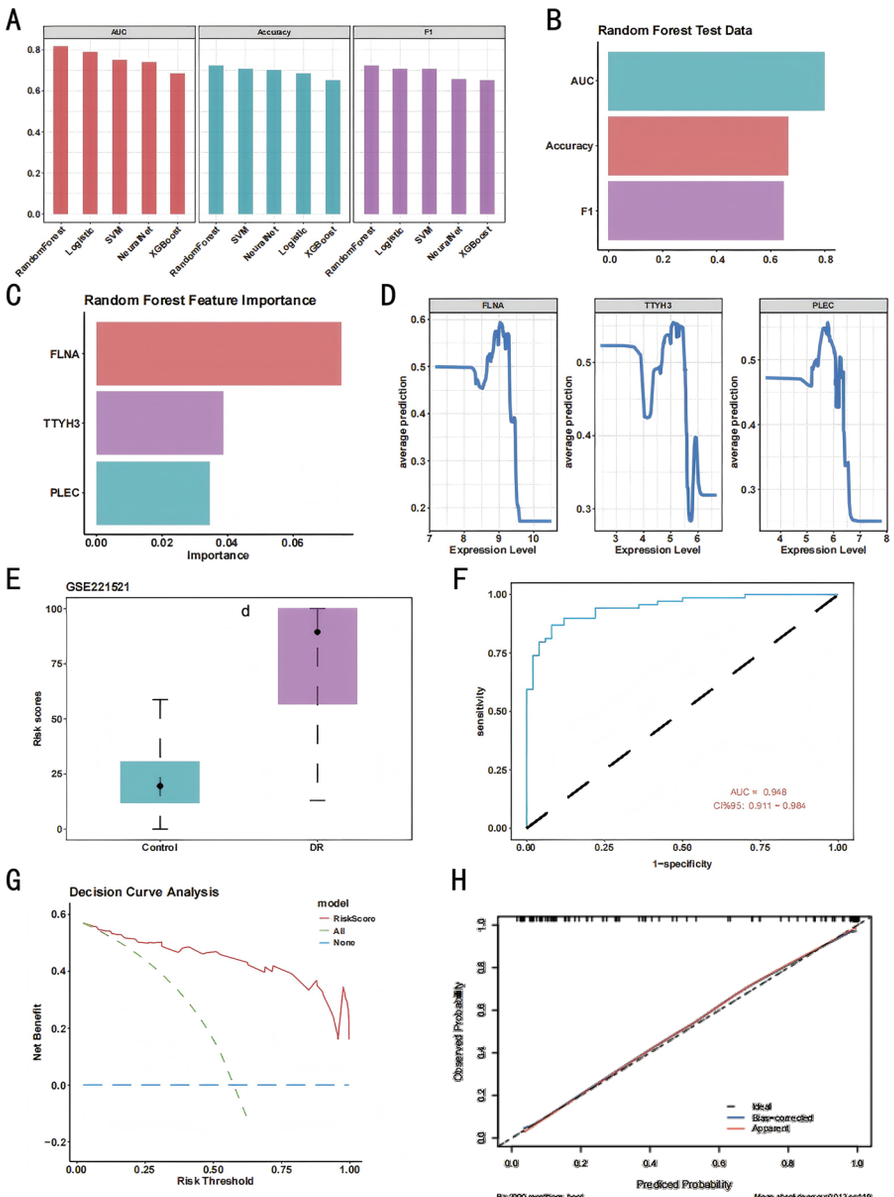

Figure 4 Multiple machine learning for intersection genes A: Model evaluation for multiple machine learning models; B: Evaluation of the Random Forest model on the test set; C: Ranking of variable importance for random forest models; D: Variable partial dependence curve of random forest model; E: Risk score distribution of GSE221521 dataset; F: Receiver operating characteristic (ROC) curve of risk score; G: Direct current analysis (DCA) curve of risk score; H: Calibration curve for risk score. ^{d}P<0.0001.

Table 2 Table of model evaluation

Model	Accuracy	AUC	F1	Sensitivity	Specificity	PPV	NPV
Logistic	0.684722	0.785238	0.703844	0.758095	0.647143	0.700714	0.67
RandomForest	0.720833	0.814683	0.721111	0.712857	0.817143	0.815	0.671667
SVM	0.705556	0.747857	0.702698	0.659524	0.825714	0.808333	0.631667
XGBoost	0.648611	0.682302	0.649185	0.64381	0.674762	0.688333	0.593333
NeuralNet	0.698611	0.737857	0.655	0.548571	0.899048	0.85	0.604048

AUC: Area under the curve; PPV: Positive predictive value; NPV: Negative predictive value; SVM: Support Vector Machine.

to the control group (Figure 4E), with a ROC curve AUC value of 0.948 (Figure 4F). Decision curve demonstrated that the red curve, representing our model, had the highest net benefit across most thresholds (0 to approximately 0.8), indicating that the model based on these three genes can assist clinicians in more accurately identifying high-risk DR patients requiring intervention (Figure 4G). Finally, the calibration curve revealed that the observed calibration curve closely aligned with the ideal 45° line, indicating good consistency between predicted and observed probabilities (Figure 4H).

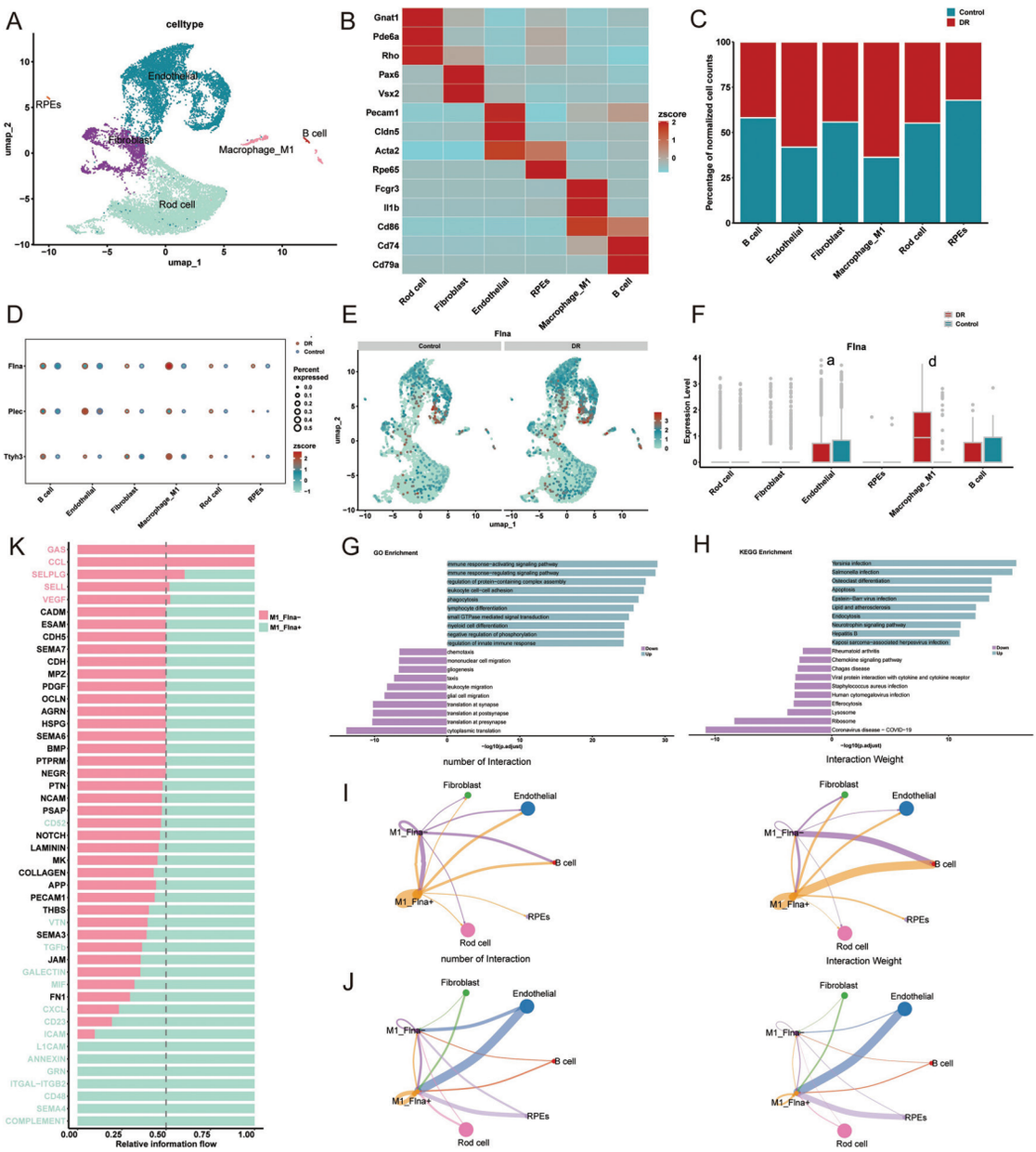

Figure 5 Single-cell sequencing analysis A: Cell annotation of the GSE243100 dataset; B: Marker gene annotation of different cell types; C: The proportion of tissue cells in the GSE243100 dataset; D: Dot plots of FLNA, PLEC, and TTYH3 expression in different cell types; E: Feature plot of FLNA expression; F: Box plot of FLNA expression differences between DR and control in different cells; G–H: GO (G) and KEGG (H) analysis of differentially expressed genes between M1_FLNA+ group and M1_FLNA- group. I–J: Cell communication analysis when M1 macrophages as source (I) or target (J); K: Relative signal flow differences between M1_FLNA+ group and M1_FLNA- group. [a]*P*<0.05, [d]*P*<0.0001. GO: Gene Ontology; KEGG: Kyoto Encyclopedia of Genes and Genomes; FLNA: Filamin A; PLEC: Plectin; TTYH3: Tweety family member 3; RPEs: Retinal pigment epithelial cells; DR: Diabetic retinopathy.

Single-cell Sequencing Analysis The preliminary results have demonstrated the high expression of key DR genes in M1 macrophages. In this section, we further investigated the expression patterns of M1 macrophages in DR samples. Through cell annotation of the GSE243100 dataset, we identified that the samples in this dataset were primarily composed of endothelial, retinal pigment epithelial cells (RPEs), fibroblast, rod cell, macrophage M1, and B cell populations (Figure 5A). By marking the marker genes of various cell types (Figure 5B), we determined the proportions of these cell types in the control and DR groups. Notably, the proportion of M1 macrophages in the DR group was significantly higher than in other cell types (Figure 5C), further validating the high expression of DR in M1 macrophages. Based on these findings, we analyzed the expression patterns of the three intersecting genes across different cell types. The expression heatmap revealed that FLNA exhibited the highest expression in M1 macrophages, followed by TTYH3, while PLEC displayed the highest expression in Endothelial cells (Figure 5D). Additionally, expression feature plots

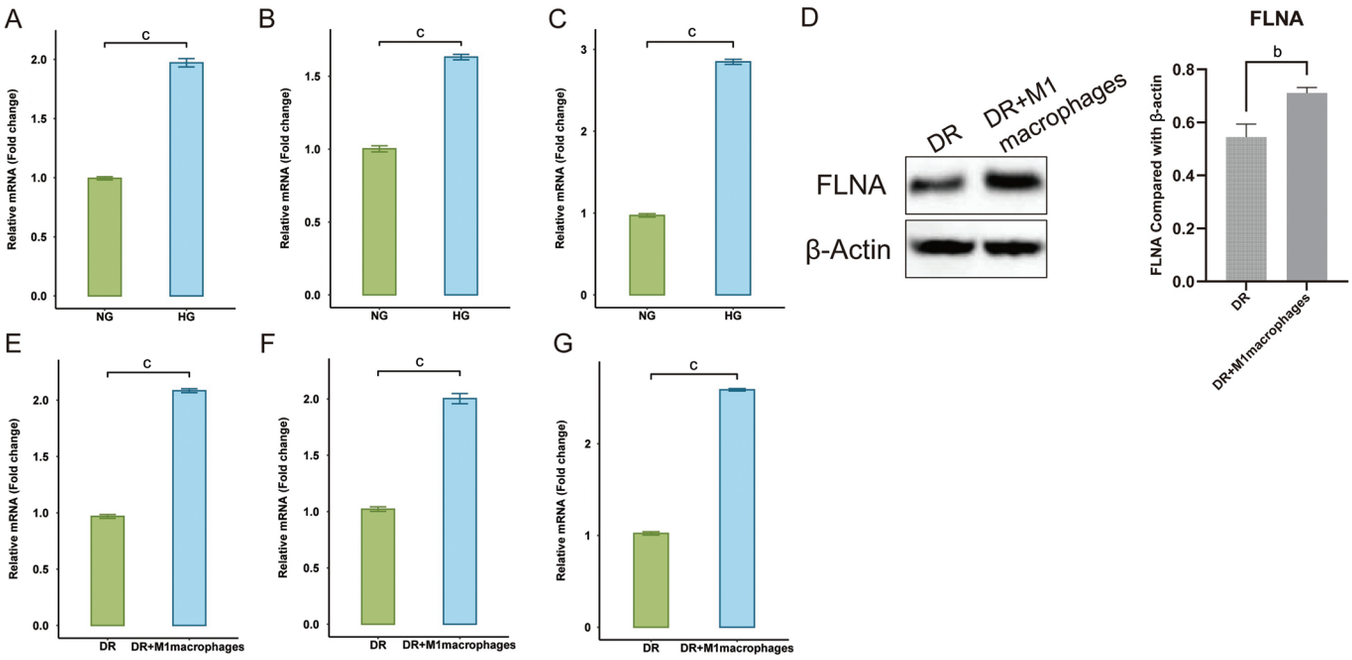

Figure 6 M1 macrophages promote the progression of DR qPCR was used to detect the mRNA expression levels of IL-6 (A), IL-1β (B) and TNF-α (C) in HG and NG. Western blotting assay to detect the protein expression level of FLNA (D). qPCR was used to detect the mRNA expression levels of IL-6 (E), IL-1β (F) and TNF-α (G) in DR and co-culturing with M1 macrophages. [b]P<0.01, [c]P<0.001. DR: Diabetic retinopathy; IL: Interleukin; TNF: Tumor necrosis factor; FLNA: Filamin A; qPCR: Quantitative real-time polymerase chain reaction; NG: Normal glucose; HG: High glucose.

and boxplots for the three genes across various cell types demonstrated that FLNA and TTYH3 exhibited the most pronounced differences in expression levels within M1 macrophages (Figure 5E–5F). Given that FLNA showed the strongest predictive importance for DR based on previous results, we prioritized FLNA for further investigation. Subsequently, we divided M1 macrophages into M1_FLNA+ and M1_FLNA- groups based on the expression of FLNA and analyzed the functional differences in their differential genes. GO analysis indicated that cells with high FLNA expression were associated with immune response or immune cell-related functions, while cells with low FLNA expression were linked to functions such as cell migration or translation (Figure 5G). KEGG analysis further revealed that high FLNA-expressing cells were associated with multiple bacterial infection diseases, whereas low FLNA-expressing cells were linked to chemokine signaling pathways or ribosome-related functions (Figure 5H). Cell communication analysis demonstrated that Endothelial cells and B cells exhibited the most frequent interactions (Figure 5I–5J). Finally, we observed that the M1_FLNA+ group exhibited higher numbers and weights of information exchange compared to the M1_FLNA- group. The differential signaling pathways between the two groups were primarily associated with molecules such as growth arrest specific (GAS), C-C motif chemokine (CCL), complement, and semaphorins 4A (SEMA4; Figure 5K).

M1 Macrophages Promote the Progression of DR To validate the previous analysis, we established a DR cell model. HRMEC cells were treated with 30 mmol/L (HG) and 5 mmol/L (NG) D-glucose, and the expression levels of DR markers IL-6, IL-1β, and TNF-α were detected using qPCR. The results showed that the expression levels of IL-6, IL-1β, and TNF-α were significantly higher in the HG group compared to the NG group (Figure 6A–6C), indicating the successful construction of the DR cell model. DR cells were co-cultured with M1 macrophages to investigate the effect of M1 macrophages on DR progression. Western blot analysis demonstrated that compared to the unco-cultured group (DR), co-culturing with M1 macrophages (DR+M1 macrophages) promoted the expression of FLNA protein (Figure 6D). qPCR results further revealed that co-culturing with M1 macrophages increased the mRNA expression levels of IL-6, IL-1β, and TNF-α compared to the unco-cultured group (Figure 6E–6G). Overall, these results suggest that M1 macrophages promote DR progression, and FLNA may contribute to the progression of DR.

FLNA Enhances the Effect of M1 Macrophages in Promoting DR In this section, we investigated the mechanism underlying the role of FLNA and M1 macrophages in the progression of DR. Initially, DR cell lines with FLNA overexpression (DR+FLNA-OE) or empty vector control (DR+vector) were established, and the efficiency of overexpression was validated *via* Western blotting (Figure

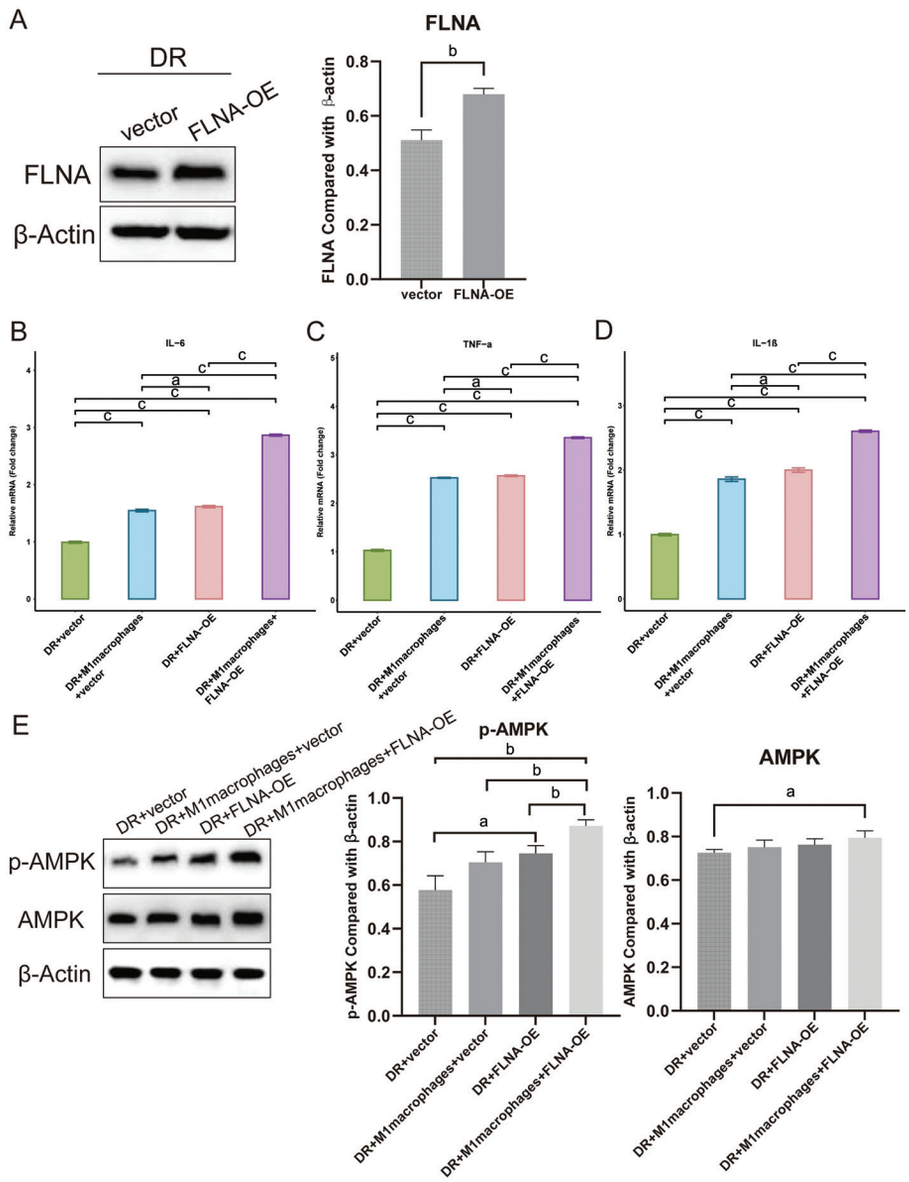

Figure 7 FLNA enhances the effect of M1 macrophages in promoting DR A: Western blotting assay to detect the overexpression efficiency of FLNA; B–D: qPCR was used to detect the mRNA expression levels of IL-6 (B), TNF-α (C) and IL-1β (D); E: Western blotting assay to detect the protein expression levels of AMPK and p-AMPK. [a]*P*<0.05, [b]*P*<0.01, [c]*P*<0.001. FLNA: Filamin A; DR: Diabetic retinopathy; IL: Interleukin; TNF: Tumor necrosis factor; qPCR: Quantitative real-time polymerase chain reaction; AMPK: AMP-activated protein kinase.

7A). Subsequently, we co-cultured FLNA-overexpressing or empty vector DR cells with M1 macrophages (DR+M1 macrophages+FLNA-OE, DR+M1 macrophages+vector). The expression levels of IL-6, IL-1β, and TNF-α were assessed using quantitative PCR. The results demonstrated that FLNA overexpression enhances the effect of M1 macrophage co-culture on increasing the expression levels of IL-6, IL-1β, and TNF-α (Figure 7B–7D). Additionally, based on the enrichment of the AMPK signaling pathway in previous FLNA KEGG analysis, we examined the levels of AMPK and its phosphorylation. The findings indicated that both FLNA overexpression and M1 macrophage co-culture increased the expression of p-AMPK protein, and FLNA overexpression further enhanced the effect of M1 macrophage co-culture on AMPK phosphorylation (Figure 7E). In conclusion, our results suggest that FLNA and M1 macrophages synergistically enhance DR progression, potentially through mechanisms involving increased AMPK phosphorylation.

DISCUSSION

The global prevalence of DR is approximately 22.27%[1,24], and its incidence among patients with DM in China is as high as 40%[25]. Therefore, improving diagnostic methods for DR and exploring its underlying mechanisms are of great significance. In this study, we integrated bulk and single-cell transcriptomics with machine learning and experimental validation to identify FLNA as a key regulator of M1 macrophage-driven DR progression, acting through AMPK phosphorylation.

In our study, we first analyzed differentially expressed genes

from the GEO database, comparing data from DR patients, normal controls, and DM patients. Through WGCNA, we identified three intersecting genes: *FLNA*, *PLEC*, and *TTYH3*. Among these, FLNA exhibited the highest predictive importance and was predominantly expressed in M1 macrophages. FLNA, an actin-crosslinking cytoskeletal protein, functions as a critical mediator of mechanotransduction and signal transduction in vascular endothelial cells and neurons[26]. Although research on FLNA in DR is still emerging, one study identified FLNA as a key hub gene in DR pathogenesis using similar approaches, such as GEO database mining and protein-protein interaction (PPI) analysis[27]. Additionally, a study demonstrated that FLNA expression was significantly upregulated in DR model mice compared to controls[28], corroborating our experimental results. Notably, recent evidence demonstrates that FLNA editing in myeloid cells reduces macrophage production of IL-6, IL-1β, and TNF-α, directly linking FLNA to macrophage inflammatory polarization[23]. Our finding that FLNA overexpression enhances M1 macrophage-mediated cytokine production in HRMECs extends this paradigm to DR, suggesting FLNA as a molecular switch amplifying M1 pro-inflammatory output.

The AMPK signaling pathway emerged as a critical node in our KEGG enrichment analysis and was experimentally validated. AMPK serves as a master regulator of cellular energy metabolism and inflammation, with its phosphorylation state dynamically governing macrophage polarization[29]. The AMPK/mTORC1 axis counterbalances M1 and M2 phenotypes: AMPK activation typically favors M2 reparative polarization, whereas mTORC1 signaling promotes M1 pro-inflammatory states. However, our results showed that FLNA and M1 macrophage co-culture increased p-AMPK levels while exacerbating inflammatory cytokine expression. This finding suggests that in the context of FLNA-overexpressing HRMECs under hyperglycemic stress, AMPK phosphorylation may be decoupled from its canonical anti-inflammatory role, potentially through FLNA-mediated scaffolding that redirects AMPK signaling toward pro-inflammatory outputs. The precise mechanism by which FLNA modulates AMPK substrate specificity in macrophage-endothelial crosstalk requires further investigation.

In recent years, the promoting role of M1 macrophages in DR has been increasingly recognized. Our experimental findings similarly demonstrate that M1 macrophages can promote the expression levels of pro-inflammatory cytokines such as IL-6, IL-1β, and TNF-α, thereby exacerbating the progression of DR. Our single-cell analysis confirmed M1 dominance in DR retinas, and co-culture experiments demonstrated that M1 macrophages promote FLNA expression and inflammatory cytokine production in HRMECs. This establishes a positive feedback loop: hyperglycemia drives M1 polarization, which upregulates FLNA, further amplifying AMPK phosphorylation and inflammatory output. Several molecules have been identified to regulate macrophage polarization, which in turn influences the progression of DR. For instance, the absence of class A scavenger receptors has been shown to promote M1 polarization of macrophages, exacerbating DR progression[30]. In addition, we found that overexpression of FLNA could further enhance the pro-inflammatory effects mediated by M1 macrophages, suggesting its potential as a therapeutic target for DR. The fat mass and obesity-associated protein (FTO) has been demonstrated to inhibit M1 polarization of macrophages by upregulating m6A modification levels, thereby mitigating DR progression[31]. Researchers have shown that IL-10 can promote M2 polarization of macrophages, improving vascular leakage and barrier disruption in the retina of diabetic mouse models[32]. Additionally, lncRNA cancer susceptibility 2 (CASC2) has been found to simultaneously suppress M1 polarization and promote M2 polarization, thereby exerting dual inhibitory effects on DR progression[33]. Therapeutically, targeting the FLNA-AMPK axis offers dual benefits: redirecting macrophage polarization while alleviating endothelial dysfunction. Nanofiber-based carriers reprogramming M1 to M2 macrophages have shown efficacy in retinal injury, suggesting that FLNA inhibition might similarly redirect macrophage phenotypes. Given FLNA's role in mechanotransduction, targeting this protein could simultaneously mitigate hyperglycemia-induced endothelial mechanical stress and inflammatory signaling[34].

In the KEGG enrichment analysis of FLNA, we identified the AMPK signaling pathway as one of the enriched signaling pathways. Subsequent experiments also demonstrated that co-culturing FLNA with M1 macrophages increased the phosphorylation levels of AMPK, suggesting that FLNA and M1 macrophages may promote the progression of DR by enhancing AMPK phosphorylation.

This study integrated public datasets and cell experiments to elucidate the significant roles of FLNA and M1 macrophages in DR, however, it lacked validation using clinical samples and *in vivo* experiments. Moving forward, we plan to conduct further investigations in clinical samples and animal models to strengthen our findings. Additionally, we have performed an initial exploration of the predictive performance of FLNA, PLEC, and TTYH3 genes for exogenous DR. Nonetheless, the current analysis is limited to public datasets and lacked validation with large-scale clinical samples, which may impact the stability and reliability of the results. To address this, we intend to further validate our findings using multicenter, large-scale clinical datasets to optimize model construction and enhance the stability and reliability of predictive performance. The precise mechanism by which FLNA scaffolds AMPK

signaling in macrophages requires structural elucidation. Future work will utilize animal models and clinical samples to validate these mechanisms and assess FLNA as a biomarker for DR risk stratification.

In conclusion, this study combined the GEO database and WGCNA analysis to identify three key genes, FLNA, PLEC, and TTYH3, and evaluated their predictive performance using machine learning. Further exploration *via* single-cell sequencing revealed the differential expression of these three genes in M1 macrophages, with FLNA exhibiting the most significant differential expression. Subsequent cellular experiments validated the promoting role of M1 macrophages and FLNA in DR progression and identified the AMPK signaling pathway as playing a critical role in the process mediated by FLNA and M1 macrophages. Our findings provide new insights into the mechanisms underlying DR development and offer novel methods for its diagnostic approaches.

ACKNOWLEDGEMENTS

Authors' Contributions: Li CH: conceptualization; methodology; investigation; writing-original draft. Feng MF: investigation; writing-review & editing. Zhang X (corresponding author): conceptualization; writing-review & editing; supervision; correspondence. Yu L: methodology; investigation; writing-review & editing. All authors have read and approved the final version of the manuscript, and confirm that no relevant contributions have been omitted or misattributed.

Data Availability Statement: The datasets generated and analyzed during the present study are available from the corresponding author on reasonable request.

AI-Generated Content Disclosure: We declare that no generative AI or AI-assisted technologies have been used in the writing, data analysis, or generation of any part of this manuscript.

Foundation: Supported by Shaanxi Provincial Science and Technology Plan Project (No.2025SF-YBXM-438).

Conflicts of Interest: Li CH, None; **Feng MF,** None; **Zhang X,** None; **Yu L,** None.

REFERENCES

1 Teo ZL, Tham YC, Yu M, *et al*. Global prevalence of diabetic retinopathy and projection of burden through 2045: systematic review and meta-analysis. *Ophthalmology* 2021;128(11):1580-1591.

2 Antonetti DA, Klein R, Gardner TW. Diabetic retinopathy. *N Engl J Med* 2012;366(13):1227-1239.

3 Wen S, Xu CL, Yuan Y, *et al*. The novel antidiabetic medications on diabetic retinopathy: relevant molecular mechanisms, advancing diagnostic innovations, and therapeutic implications. *Front Med (Lausanne)* 2026;12:1670643.

4 Wells JA, Glassman AR, Ayala AR, *et al*. Aflibercept, bevacizumab, or ranibizumab for diabetic macular edema: two-year results from a comparative effectiveness randomized clinical trial. *Ophthalmology* 2016;123(6):1351-1359.

5 Bressler NM, Beaulieu WT, Glassman AR, *et al*. Persistent macular thickening following intravitreous aflibercept, bevacizumab, or ranibizumab for central-involved diabetic macular edema with vision impairment: a secondary analysis of a randomized clinical trial. *JAMA Ophthalmol* 2018;136(3):257-269.

6 Jaffe GJ, Westby K, Csaky KG, *et al*. C5 inhibitor avacincaptad pegol for geographic atrophy due to age-related macular degeneration a randomized pivotal phase 2/3 trial. *Ophthalmology* 2021;128(4):576-586.

7 Sahni J, Patel SS, Dugel PU, *et al*. Simultaneous inhibition of angiopoietin-2 and vascular endothelial growth factor-a with faricimab in diabetic macular edema: boulevard phase 2 randomized trial. *Ophthalmology* 2019;126(8):1155-1170.

8 Yao YJ, Li JJ, Zhou YF, *et al*. Macrophage/microglia polarization for the treatment of diabetic retinopathy. *Front Endocrinol (Lausanne)* 2023;14:1276225.

9 Hu AY, Schmidt MHH, Heinig N. Microglia in retinal angiogenesis and diabetic retinopathy. *Angiogenesis* 2024;27(3):311-331.

10 Tang J, Kern TS. Inflammation in diabetic retinopathy. *Prog Retin Eye Res* 2011;30(5):343-358.

11 Adamis AP. Is diabetic retinopathy an inflammatory disease? *Br J Ophthalmol* 2002;86(4):363-365.

12 Murray PJ, Allen JE, Biswas SK, *et al*. Macrophage activation and polarization: nomenclature and experimental guidelines. *Immunity* 2014;41(1):14-20.

13 Liu WF, Tong B, Xiong J, *et al*. Identification of macrophage polarisation and mitochondria-related biomarkers in diabetic retinopathy. *J Transl Med* 2025;23(1):23.

14 Xu ZK, Wu YB, Mao JB, *et al*. 4D label-free proteomics analysis of oxygen-induced retinopathy with or without anti-VEGF treatment. *BMC Genomics* 2024;25(1):415.

15 Wang S, Zheng YX, Li JY, *et al*. Single-cell transcriptomic atlas of primate ovarian aging. *Cell* 2020;180(3):585-600.e19.

16 Orecchioni M, Ghosheh Y, Pramod AB, *et al*. Macrophage polarization: different gene signatures in M1(LPS+) *vs*. classically and M2(LPS-) *vs*. alternatively activated macrophages. *Front Immunol* 2019;10:1084.

17 Li J, Yu SS, Lu X, *et al*. The phase changes of M1/M2 phenotype of microglia/macrophage following oxygen-induced retinopathy in mice. *Inflamm Res* 2021;70(2):183-192.

18 Hu J, Dziumbla S, Lin JH, *et al*. Inhibition of soluble epoxide hydrolase prevents diabetic retinopathy. *Nature* 2017;552(7684):248-252.

19 Wang YL, Lin QS, Zhang H, *et al*. M2 macrophage-derived exosomes promote diabetic fracture healing by acting as an immunomodulator. *Bioact Mater* 2023;28:273-283.

20 Rönty MJ, Leivonen SK, Hinz B, *et al*. Isoform-specific regulation of the actin-organizing protein palladin during TGF-beta1-induced myofibroblast differentiation. *J Invest Dermatol* 2006;126(11):2387-2396.

21 Guijarro-Muñoz I, Compte M, Álvarez-Cienfuegos A, *et al*. Lipopolysaccharide activates Toll-like receptor 4 (TLR4)-mediated NF-κB signaling pathway and proinflammatory response in human pericytes. *J Biol Chem* 2014;289(4):2457-2468.

22 Viollet B, Horman S, Leclerc J, *et al*. AMPK inhibition in health and disease. *Crit Rev Biochem Mol Biol* 2010;45(4):276-295.

23 Gawish R, Varada R, Deckert F, *et al*. Filamin A editing in myeloid cells reduces intestinal inflammation and protects from colitis. *J Exp Med* 2025;222(9):e20240109.

24 Chen ZG, Liu GQ, Liu WM, *et al*. Inhibition of viability of human retinal microvascular endothelial cells by vialinin A under high glucose condition. *Int J Ophthalmol* 2024;17(10):1809-1815.

25 Yin L, Zhang DL, Ren Q, *et al*. Prevalence and risk factors of diabetic retinopathy in diabetic patients: a community based cross-sectional study. *Medicine* 2020;99(9):e19236.

26 Zhou J, Kang XM, An HX, *et al*. The function and pathogenic mechanism of filamin A. *Gene* 2021;784:145575.

27 Abbasi sani B, Ahmad S, Abu Omaima HAA, *et al*. Investigation of aldose reductase inhibitors: implications for therapeutic targets in diabetic retinopathy. *J Mol Struct* 2025;1336:142004.

28 Vähätupa M, Nättinen J, Jylhä A, *et al*. SWATH-MS proteomic analysis of oxygen-induced retinopathy reveals novel potential therapeutic targets. *Invest Ophthalmol Vis Sci* 2018;59(8):3294-3306.

29 Yang Z, Kahn BB, Shi H, *et al*. Macrophage alpha1 AMP-activated protein kinase (alpha1AMPK) antagonizes fatty acid-induced inflammation through SIRT1. *J Biol Chem* 2010;285(25):19051-19059.

30 Ma K, Xu YM, Wang CC, *et al*. A cross talk between class A scavenger receptor and receptor for advanced glycation end-products contributes to diabetic retinopathy. *Am J Physiol Endocrinol Metab* 2014;307(12):E1153-E1165.

31 Feng SG, Zhang QY, Liu Q, *et al*. N 6-methyladenosine demethylase FTO controls macrophage homeostasis in diabetic vasculopathy. *Diabetes* 2025;74(1):82-95.

32 Lee SJ, Noh SE, Jo DH, *et al*. IL-10-induced modulation of macrophage polarization suppresses outer-blood-retinal barrier disruption in the streptozotocin-induced early diabetic retinopathy mouse model. *FASEB J* 2024;38(9):e23638.

33 Xiao F, Wu FP, Zhong PP, *et al*. LncRNA CASC2 mediates SOCS6 mRNA stabilization *via* U2AF2 recruitment to modulate macrophage polarisation in diabetic retinopathy. *Diabet Med* 2025;42(8):e70014.

34 Zhang ZH, Peng SJ, Xu TY, *et al*. Retinal microenvironment-protected Rhein-GFFYE nanofibers attenuate retinal ischemia-reperfusion injury *via* inhibiting oxidative stress and regulating microglial/macrophage M1/M2 polarization. *Adv Sci* (*Weinh*) 2023;10(30):e2302909.